

---

# SHARE-SSM: AN OSCILLATORY SPIKING NEURAL NETWORK FOR TARGET VARIABLE MODELING IN LONG SEQUENCES

---

Kartikay Agrawal<sup>1</sup>, Abhijeet Vikram<sup>2</sup>, Vedant Sharma<sup>2</sup>, Vaishnavi N.<sup>1</sup>, Ayon Borthakur<sup>1</sup>

<sup>1</sup>SustainAI Lab, MFSDSAI, IIT Guwahati, Assam, India, 781039

<sup>2</sup>IISER Pune, Maharashtra, India, 411008

{a.kartikay,n.vaishnavi,ayon.borthakur}@iitg.ac.in  
{vedant.sharma,abhijeet.vikram}@students.iiserpune.ac.in

## ABSTRACT

In recent years, with the emergence of large models, there has been a significant interest in spiking neural networks (SNNs) primarily due to their energy efficiency, multiplication-free, and sparse event-based deep learning. Similarly, state space models (SSMs) in varying designs have evolved as a powerful alternative to transformers for target modeling in long sequences, thereby overcoming the quadratic dependence on sequence length of a transformer. Inspired by this progress, we here design SHaRe-SSM (Spiking Harmonic Resonate and Fire State Space Model), for target variable modeling (including both classification and regression) for very-long-range sequences. Our second-order spiking SSM, on average, performs better than transformers or first-order SSMs while circumventing multiplication operations, making it ideal for resource-constrained applications. The proposed block consumes  $73\times$  less energy than second-order ANN-based SSMs for an 18k sequence, while retaining performance. To ensure learnability over the long-range sequences, we propose exploiting the stable and efficient implementation of the dynamical system using parallel scans. Moreover, for the first time, we propose a kernel-based spiking regressor using resonate and fire neurons for very long-range sequences. Our network shows superior performance on even a 50k sequence while being significantly energy-efficient. In addition, we conducted a systematic analysis of the impact of heterogeneity, dissipation, and conservation in resonate-and-fire SSMs.

## 1 Introduction

Spike-based deep learning is a well-established approach for efficient Artificial Intelligence, especially due to its traits of ultra-low energy consumption and sparse computation. Whether it is digital spiking neuromorphic hardware such as Loihi [1, 2], TrueNorth [3], or analog neuromorphic hardware such as Dynapse [4], the spike-based computation resource utilization is significantly lower than artificial neural networks.

Presently, a significant amount of these spike-based deep learning [5, 6, 7, 8, 9] focus on using simple integrate and fire (IF) neurons (or their leaky version (LIF)). Although IF neurons are biologically plausible, they miss key biological characteristics such as oscillatory dynamics. Such rich dynamics are observed empirically and in biophysically detailed Hodgkin-Huxley (HH) models [10]. Although the HH model provides an accurate and detailed representation of neuronal dynamics, its high computational cost makes it impractical for large-scale AI systems. But Resonate and Fire (RF) neurons [11], though computationally equivalent to IF neurons, are expressive enough to capture such rich dynamics of biological neurons. Hence, recently, there has been a significant interest in designing RF-based spiking neural networks [2, 12, 13]. To the best of our knowledge, RF neurons have not been studied in a very long sequence for target variable modeling (classification as well as regression).

For sequential data processing, transformers are the de facto standard [14]. But a vanilla transformer requires quadratic computational complexity with respect to the sequence length. To obviate these limitations, methods like KV caching [15] or test-time memory updates [16] have been proposed. However, they do not match the computational simplicity of recurrent neural networks (RNNs). Hence, there has been significant interest in designing SSMs [17, 18, 19], including

spiking neurons [9, 8, 20], which promise to get the best of both transformers and RNNs. But the existing spiking SSMs are not optimal for target variable modeling in very long sequences.

Furthermore, as detailed in [21], it’s very difficult to select a state matrix for very long interactions in a first-order SSM. To overcome these constraints, they proposed LinOSS, which is a second-order state space model [21, 22]. Interestingly, LinOSS attains high classification for extremely long sequence classification and regression only with a diagonal state matrix. It achieves this by leveraging stable discretizations whose spectral radius stays close to one. LinOSS is state-of-the-art in performance on extremely long-range interactions. However, it lacks key biological features, such as spike-based communication, which has also been shown to demonstrate superior energy benefits in AI applications [2, 23].

Inspired by this progress, in this work, we propose SHaRe-SSM: Spiking Harmonic Resonate and Fire State Space Model, a second-order spike-based SSM primarily targeted for extremely long-range performance. Due to spike-based computation, SHaRe-SSM is energy efficient and hence is ideal for resource-constrained applications, such as in always-on edge AI devices. In summary, our work makes the following contributions:

- We propose and rigorously evaluate a second-order spiking SSM: SHaRe-SSM. Noteworthy, unlike some of the previous first-order SSMs [20, 8, 9], SHaRe-SSM is completely spike-based without using non-linearities such as GeLU, GLU, or GSU.
- As part of it, for rapid training and inference, we propose a compatible parallel scan algorithm.
- Furthermore, we observe that SHaRe-SSM outperforms all first-order SSMs on very long sequence classification. And, SHaRe-SSM is significantly energy efficient than ANN-based second-order SSMs.
- Also, we extend SHaRe-SSM to energy-efficient long-range regression applications and propose a convolving kernel-based regression. We observe that SHaRe-SSM outperforms first-order SSMs on a 50K sequence length regression task.
- Finally, we study and explore the impact of discretization methods and network heterogeneities on SHaRe-SSM.

## 2 Related Works

**State Space Models:** Structured State Space Models (SSMs), including S4, Mamba, and LRU, have demonstrated state-of-the-art performance on a wide range of sequence modeling tasks, particularly in language modeling [19] and time series forecasting [21]. These models leverage the mathematical structure of state space representations to model long-range dependencies efficiently and scalably [17, 18, 24]. Recent work shows that neural oscillators, as universal function approximators, naturally capture long-range temporal dependencies and often outperform traditional models [25, 26, 27]. They benefit from numerically stable Implicit-Explicit (IMEX) and Implicit Euler (IM) discretizations, which better handle complex dynamics than standard Explicit Euler methods. LinOSS [21] builds on this oscillator-based perspective, proposing a linear implicit oscillator-based state-space model that combines the stability of implicit solvers with the expressivity of neural oscillatory dynamics. This leads to better inductive biases for learning long sequences, especially when capturing slow or multi-scale temporal phenomena. However, LinOSS is not optimal for resource-constrained applications (such as in edge AI) due to its computational complexity.

**Spiking Neural Networks:** Spiking Neural Networks (SNNs) form a biologically inspired class of neural models characterized by discrete spike-based communication. The most foundational models include the IF, LIF neurons. These have been extended to include adaptation mechanisms, such as in Adaptive LIF (ALIF), and more complex dynamics as in the RF [11] and Harmonic Resonate-and-Fire (HRF) [28] neurons. Many ALIF-based recurrent models have been proposed [29, 30, 31], with recent works extending adaptation to RF and HRF neurons [28, 12], which have been evaluated on only small sequence datasets. SNNs are increasingly modeled within the SSM framework for efficient computation, especially on resource-constrained hardware. [13] reformulated LIF and RF neurons as SSMs following [30], achieving strong results on neuromorphic benchmarks. Yet, scaling to extremely long-range sequences remains a key challenge. Recent non-adaptive, first-order SSM-based spiking models such as S4D-/S4-inspired LIF neurons [9, 20, 8] and RF-based variants [32] perform well on mid-range tasks (up to 16k sequence length) but fall short on longer sequences. Notably, none have been evaluated on extremely long-range time series or regression benchmarks. While an FFT-based transformer [33] has been introduced for regression, its reliance on computationally heavy FFTs limits suitability for neuromorphic deployment [20]. [34] recently validated the efficacy of an S4D-based spiking SSM by implementing it on Loihi 2. Although this design was efficient, it was evaluated on reasonably simple sCIFAR-10 datasets only.

[35, 36] showed that in LIF/IF-based networks, neural heterogeneity—variation in neuron hyperparameters can improve classification performance. In SHaRe-SSM, we aim to explore this further by focusing on HRF neurons in a second-order SSM framework, thereby investigating the combined effects of heterogeneity and discretization. Most prior studies have relied on explicit discretization schemes, with very few exploring alternatives. A notable exception is [37], which demonstrated improved performance using a symplectic implicit-explicit (IMEX) scheme over conventional adaptive-LIF models [30]. We here focus on enhancing the expressivity of HRF neurons by integrating them into a fully spike-based SSM framework (SHaRe-SSM).

### 3 Methods

#### 3.1 Network Description

The Resonate-and-Fire (RF) neuron, introduced by [11], better approximates the Hodgkin-Huxley (HH) model than the Leaky Integrate-and-Fire (LIF) neuron. This is because it captures complex-valued subthreshold dynamics using a 2D linear system with a complex eigenvalue, enabling membrane resonance and frequency preference. Unlike the purely real-valued LIF neuron, RF can exhibit oscillatory behavior and selective amplification of certain input frequencies, features also observed in HH neurons. Later, second-order real-valued approximations, e.g., [28, 12], simplify RF into a real harmonic-oscillator-like form often referred to as HRF. HRF preserves oscillatory behavior via complex eigenvalues similar to the RF neuron, but without requiring initialization in complex space; The RF model’s inherent complex dynamics are a key reason it is considered more biophysically realistic. Recently, [12] showed RF-based models work best without resetting the membrane potential. After collating these observations, we here integrate HRF into an SSM framework and compute neuronal dynamics linearly using parallel scans, and use the spike function as an activation function to propagate spikes.

A Harmonic-Resonate-and-Fire Neuron is defined by:

$$\begin{aligned}
 u'(t) &= -\omega^2 v(t) - 2bu(t) + x(t) \\
 v'(t) &= u(t) \\
 z(t) &= \Theta(u(t) - \theta)
 \end{aligned}
 \tag{1}$$

where  $v(t)$  denote the hidden state,  $u(t)$  as the time derivative of  $v(t)$ ,  $x(t)$  is the input spikes to the neuron,  $\omega \in \mathbb{R}$  is the frequency parameter and  $b \in \mathbb{R}$  is the damping coefficient. Spiking Function:  $\Theta \in \{0, 1\}$  i.e. spikes are emitted if  $u \geq \theta$ .

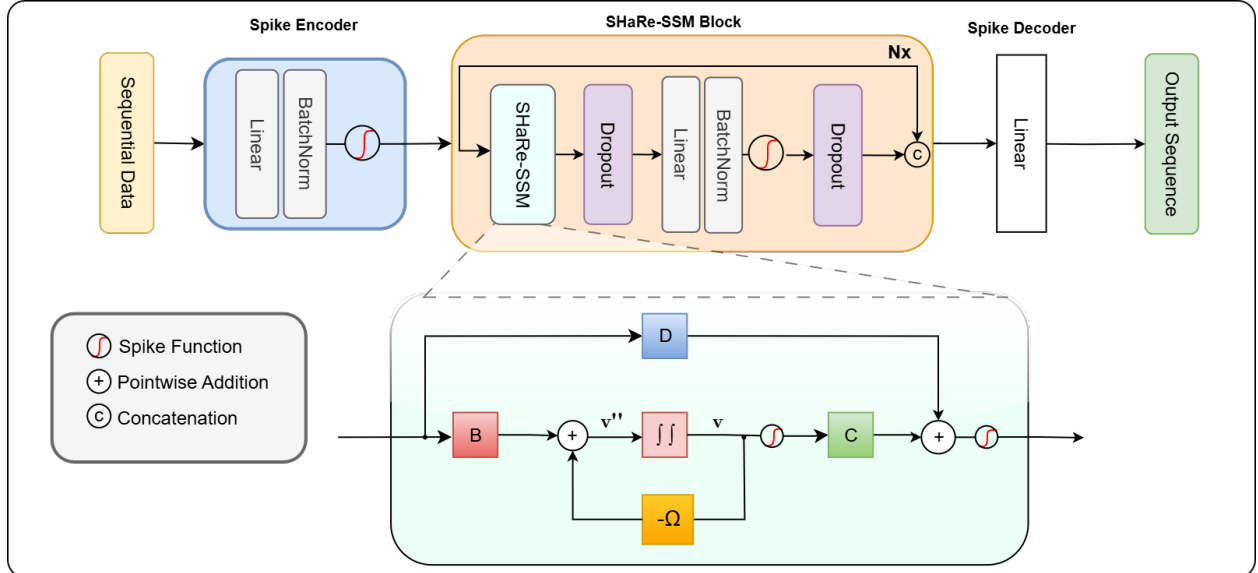


Figure 1: Description of SHaRe-SSM model. SHaRe-SSM consists of a SHaRe-SSM neuron representing multiple states (Eq. 1) followed by a Linear layer repeated for N blocks. Spikes are encoded with a Spike Encoder and decoded using a Spike Decoder.

This HRF formulation is limited to a single neuron. We propose formulating HRF in an SSM framework (SHaRe-SSM). This approach helps in capturing better dynamics. The input spikes are multiplied by a weight matrix, and we propagate

spikes from the hidden state  $v(t)$ . Moreover, removing the damping parameter in such second-order approximations enhances the neuron’s ability to capture long-range temporal dependencies by preserving longer oscillations [21]. We define the SHaRe-SSM model by:

$$\begin{aligned}
 u'(t) &= -\Omega v(t) + Bx(t) \\
 v'(t) &= u(t) \\
 z(t) &= \Theta(v(t) - \theta) \\
 y(t) &= Cz(t) + Dx(t)
 \end{aligned}
 \tag{2}$$

where  $u(t), v(t) \in \mathbb{R}^p$  denote the hidden states,  $y(t) \in \mathbb{R}^h$  the output, and  $x(t) \in \mathbb{R}^h$  the input spike signal. The system is defined by weights  $\Omega \in \mathbb{R}^{p \times p}$  which is diagonal,  $B \in \mathbb{R}^{p \times h}$ ,  $C \in \mathbb{R}^{h \times p}$ ,  $D \in \mathbb{R}^h$ , and an output learnable spiking parameter  $\theta \in \mathbb{R}^p$  such that spikes are emitted if  $v \geq \theta$ . These thresholds ( $\theta$ ) are learned using a step-double Gaussian surrogate gradient [38, 12]. Since [12] showed that HRF works well with no reset, we here employed the same strategy. This avoids the need for sequential processing, and the model can be implemented across time as an activation function. Figure 1 describes the SHaRe-SSM design. Each SHaRe-SSM block is comprised of SHaRe-SSM neuron, followed by a linear layer, batch normalization, and an IF neuron. We mix spikes from the previous layer and introduce dropout layers to avoid learnable thresholds from saturating early. SHaRe-SSM uses only binary spike-based communication between blocks.

### 3.2 Encoder and Decoder

For SHaRe-SSM, we design an encoder for encoding the input signal into spike trains (see Figure 1). Herein, the inputs every timestep are passed through a learnable linear layer. The output of this layer is passed through a batch normalization layer. Finally, an IF neuron generates spikes into the SHaRe-SSM block. Notably, this is a data-dependent trainable encoder (without requiring us to specify whether to utilize rate coding or any other encoding variants). Moreover, it utilizes neuronal heterogeneity and is instantaneous.

The decoder projects the spikes back using a linear Layer with the output dimension equal to the number of classes. For regression, we also propose convolving the output with a learnable filter.

### 3.3 Discretization methods

For understanding the impact of discretization on an HRF neuron (Eq. 1), we conduct a single neuron simulation (Figure 2) by injecting a unit spike input to an HRF neuron with zero phase. For the continuous case, if the damping parameter 'b' is constrained to be non-negative, we must get stable dynamics. If set to zero, we should observe sustained oscillation. From Figure 2, we can see that for Euler Forward (Explicit), our model is diverging over time, making it unstable. IMEX discretization is overall stable and hence preserves energy. IM, although dissipative in energy, is still stable. We briefly describe IM and IMEX generalizability for long sequences in detail below.

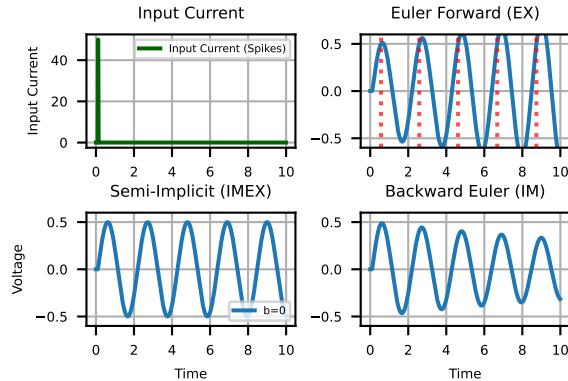


Figure 2: Post-spike membrane potential behavior for a Harmonic RF neuron for different discretizations with no damping. The dotted red line denotes the inter-spike interval.

IMEX is promising, as [21] showed that removing damping leads to a Hamiltonian system [39], where energy conservation is ensured under symplectic discretizations. In addition, we examine the non-conservative but stable IM scheme, which performs well empirically. We adopt a second-order system with position-like state  $u_n$  and velocity-like

state  $v_n$ . The general form of discrete updates is denoted by:

$$u_n = u_{n-1} + \Delta t(-\Omega v_* + Bx_n), \quad (3)$$

$$v_n = v_{n-1} + \Delta t u_n, \quad (4)$$

$$s_n = Ms_{n-1} + F_n, \quad (5)$$

where the choice of  $v_*$  distinguishes the discretization schemes:  $v_* = v_n$  for IM (implicit), and  $v_* = v_{n-1}$  for IMEX (implicit-explicit).

For the IM scheme, we define [21]:

$$M^{\text{IM}} = \begin{pmatrix} S & -S\Delta t\Omega \\ S\Delta t & S \end{pmatrix}, \quad F_n^{\text{IM}} = \begin{pmatrix} S\Delta t Bx_n \\ S\Delta t^2 Bx_n \end{pmatrix},$$

with  $S = (I + \Delta t^2\Omega)^{-1}$ , acting as a Schur complement that suppresses high-frequency components and ensures eigenvalues of  $M^{\text{IM}}$  remain bounded within the unit circle.

And, for the IMEX scheme, we use [21]:

$$M^{\text{IMEX}} = \begin{pmatrix} I & -\Delta t\Omega \\ \Delta t I & I - \Delta t^2\Omega \end{pmatrix}, \quad F_n^{\text{IMEX}} = \begin{pmatrix} \Delta t Bx_n \\ \Delta t^2 Bx_n \end{pmatrix}.$$

Unlike IM, the eigenvalues of  $M^{\text{IMEX}}$  lie near the unit circle, preserving oscillatory energy over long horizons. This makes IMEX especially suitable for modeling long sequences, where maintaining temporal structure is crucial.

### 3.4 Parallel scan in SHaRe-SSM

Parallel scans [40, 41] exploit associativity to reduce the time complexity of recurrent computations from  $\mathcal{O}(N)$  to  $\mathcal{O}(\log N)$ . Originally developed to accelerate RNNs, they have recently been adapted for state-space models [18], powering modern architectures like Linear Recurrent Units (LRUs) [24] and Mamba [19]. Leveraging this structure allows for richer exploration of neuronal state trajectories and improves training efficiency. We apply parallel scans to the linear computations, followed by spike function activations.

An associative binary operation similar to [21] defined as:

$$(a_1, a_2) \bullet (b_1, b_2) = (b_1 \cdot a_1, b_1 \cdot a_2 + b_2),$$

where  $\cdot$  represents matrix-matrix and matrix-vector multiplications. Applying a parallel scan to the input sequence  $[(M, F_1), (M, F_2), \dots]$  efficiently computes the solution to the  $s_n = Ms_{n-1} + F_n$ . The scan output stores  $x_n$  in the second element of each tuple. This is made efficient by exploiting structured matrices (e.g., diagonal block  $2 \times 2$  matrices in  $M_{\text{IM}}$  and  $M_{\text{IMEX}}$ ), where each product can be computed in linear time with respect to the hidden dimension. We use this approach to leverage IMEX and IM discretization schemes on an HRF neuron. Algorithm 1 describes our SHaRe-SSM implementation.

---

#### Algorithm 1 SHaRe-SSM Algorithm

---

**Require:** Input sequence  $x$

**Ensure:**  $N$ -blocks, spike function  $\Theta$ , output sequence  $o$

$x^0 \leftarrow \text{Encoder}(x)$  {Encode input sequence into spikes}

**for**  $n = 1, \dots, N$  **do**

$z^n \leftarrow$  solution of HRF in (2) with input  $x^{n-1}$  via parallel scan aggregated

$z^n \leftarrow \Theta(y^n - \theta_C^n)$

$y^n \leftarrow Cz^n + Dx^{n-1}$  {Weighted spike mixing in (2)}

$y^n \leftarrow \text{drop}(\Theta(y^n - \theta_D^n))$

$y^n \leftarrow \text{Linear}(y^n)$

$y^n \leftarrow \text{BN}(y^n)$

$y^n \leftarrow \text{drop}(\Theta(y^n - \theta^n))$

$x^n \leftarrow \text{cat}(x^{n-1}, y^n)$

**end for**

$o \leftarrow \text{Decoder}(x^N)$  {Decode spikes}

---

Table 1: Classification performance (mean and standard deviation across five training runs) for UEA time-series datasets using hyperparameter protocol from [42]. For convenience, some dataset names are abbreviated: Worms (EigenWorms), SCP1 (SelfRegulationSCP1), SCP2 (SelfRegulationSCP2), Ethanol (EthanolConcentration), Heartbeat, and Motor (MotorImagery). The top two models are bold and underlined, respectively. SNN implies a spiking neural network(Y/N).

Seq. Length/ Class	SNN	17,984/5 <b>Worms</b>	896/2 <b>SCP1</b>	1,152/2 <b>SCP2</b>	1,751/4 <b>Ethanol</b>	405/2 <b>Heartbeat</b>	3,000/2 <b>Motor</b>	Avg
NRDE	N	83.9 ± 7.3	80.9 ± 2.5	53.7 ± 6.9	25.3 ± 1.8	72.9 ± 4.8	47.0 ± 5.7	60.6
NCDE	N	75.0 ± 3.9	79.8 ± 5.6	53.0 ± 2.8	29.9 ± 6.5	73.9 ± 2.6	49.5 ± 2.8	60.2
Log-NCDE	N	85.6 ± 5.1	83.1 ± 2.8	53.7 ± 4.1	<b>34.4 ± 6.4</b>	75.2 ± 4.6	53.7 ± 5.3	64.3
LRU	N	87.8 ± 2.8	82.6 ± 3.4	51.2 ± 3.6	21.5 ± 2.1	<b>78.4 ± 6.7</b>	48.4 ± 5.0	61.7
S5	N	81.1 ± 3.7	<b>89.9 ± 4.6</b>	50.5 ± 2.6	24.1 ± 4.3	77.7 ± 5.5	47.7 ± 5.5	61.8
S6	N	85.0 ± 16.1	82.8 ± 2.7	49.9 ± 9.4	26.4 ± 6.4	76.5 ± 8.3	51.3 ± 4.7	62.0
Mamba	N	70.9 ± 15.8	80.7 ± 1.4	48.2 ± 3.9	27.9 ± 4.5	76.2 ± 3.8	47.7 ± 4.5	58.6
LinOSS (IM)	N	<b>95.0 ± 4.4</b>	87.8 ± 2.6	58.2 ± 6.9	29.9 ± 0.6	75.8 ± 3.7	60.0 ± 7.5	67.8
LinOSS (IMEX)	N	80.0 ± 2.7	87.5 ± 4.0	<b>58.9 ± 8.1</b>	29.9 ± 1.0	75.5 ± 4.3	57.9 ± 5.3	65.0
D-LinOSS	N	93.9 ± 3.2	88.9 ± 3.0	58.6 ± 2.3	29.9 ± 0.6	75.8 ± 4.9	<b>61.1 ± 2.0</b>	<b>68.0</b>
<b>Ours (IM)</b>	Y	85.6 ± 8.1	82.6 ± 4.5	<b>55.4 ± 6.9</b>	30.1 ± 1.47	<b>74.1 ± 5.9</b>	<b>59.6 ± 5.4</b>	<b>64.4</b>
Ours (IMEX)	Y	<b>85.6 ± 2.7</b>	<b>82.6 ± 4.2</b>	53.0 ± 4.8	<b>32.4 ± 4.6</b>	73.2 ± 5.73	58.6 ± 7.3	64.2

## 4 Empirical Results

### 4.1 Long-range sequence classification

For classification experiments, we show SHaRe-SSM’s efficacy on the long-range sequential benchmark introduced in [42, 21] with pre-selected random seeds for splitting the dataset (70/15/15 splits) and a fixed model hyperparameter range. It consists of the six longest sequence datasets pertaining to real-world applications from the University of East Anglia Multivariate Time Series Classification Archive (UEA-MTSCA) [43]. To the best of our knowledge, SHaRe-SSM is the first second-order spiking SSM proposed. In addition, the recently proposed ANN-based second-order SSM (LinOSS) [21] very clearly establishes its superiority over first-order SSMs. Moreover, presently proposed spiking first-order SSM’s performance [20, 8, 9] is bounded by S4D’s performance. Hence, for these extremely long-range classification tasks, we compare our model performance only to the ANN-based State Space Models[18, 19, 21] (First and Second order) and Neural controlled ODEs[44, 45, 42] only. ANN-based LinOSS [21] leverages second-order ODEs for long-range sequence learning and outperforms other SOTA models on such very long-range benchmark datasets. Similarly, SHaRe-SSM, on average, performs better than Mamba & S6 by 5.7% & 2.3% (See Table 1 respectively, while being only 3.6% lower than SOTA D-LinOSS. Our simplistic but fully spike-based model design (SHaRe-SSM), which leverages HRF neuronal dynamics, performs just 9.4% lower than LinOSS for IM discretization on the 18k Eigenworms dataset (noteworthily [20] also observed a 9.4% performance drop on the Pathfinder dataset when compared to S4). Whereas for IMEX discretization, SHaRe-SSM outperforms LinOSS by 5.6%, while being extremely energy efficient (see Table 1). Moreover, we notice a trend that even though accuracy is the same, IMEX standard deviation is lower by 5.41% and 0.32% than IM for EigenWorms and SCP1, respectively. This strengthens the claim that IM introduces dissipative terms that can impact model performance. Similarly, we observe that for the Ethanol data set, the IMEX discretization on SHaRe-SSM outperforms all variants of LinOSS by 2.5%. While Log-NCDE outperforms our model, it comes with its own ODE computational overheads compared to LinOSS. On the 3k MotorImagery dataset, SHaRe-SSM achieves a performance of 59.6% (vs. 61.1% for D-LinOSS). Overall, our second-order spiking SSM outperforms first-order SSMs based on Mamba. Notably, a drop in performance with the gain in efficiency is ubiquitous across spiking SSMs for LRA tasks [9, 20, 8]. To ensure a fair comparison, we followed the hyperparameter protocol from [42]; However, constrained by computational resources and time, instead of grid search, we ran Bayesian search using Optuna [46] for 15 runs and performed a narrow search.

#### 4.1.1 Energy computation

In this section, we assess and compare the energy computation for LinOSS and SHaRe-SSM for similar hidden-size(H), state-size(P), and num-blocks(N) on the EigenWorms dataset. We estimate the theoretical energy consumption of our model based on prior works [8, 20, 33]. Accordingly, we assume that MAC and AC operations are implemented on a 45nm hardware [47], where  $E_{MAC} = 4.6\text{pJ}$  and  $E_{AC} = 0.9\text{pJ}$ . Notably, as discussed in [8], the computational cost of multiplication of a floating-point weight by a binary activation number is represented as an addition-only operation. For ANNs, the theoretical energy consumption of a block  $n$  is given by  $4.6\text{pJ} \times \text{FLOPs}(n)$ . For SNNs, the energy consumption for  $n$  is given by  $0.9\text{pJ} \times \text{SOPs}(n)$ . Calculating theoretical energy consumption requires

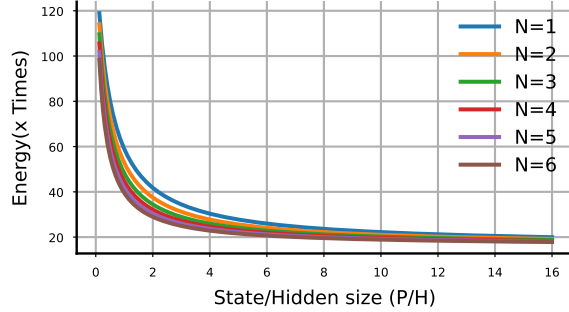


Figure 3: Variation of energy computation of a LinOSS Block [21] to the SHaRe-SSM Block for EigenWorms with respect to State (P), Hidden size (H).

first calculating the synaptic operations,  $SOPs(n) = f_r \times FLOPs(n)$ ,  $f_r$  is the firing rate of the input spike train of the block/layer,  $FLOPs(n)$  refers to the number of floating-point operations in layer  $n$ , equivalent to the number of multiply-and-accumulate (MAC) operations. SOPs denote the number of spike-based accumulate (AC) operations.

Since  $\Omega$  is a diagonal matrix, it can be efficiently implemented using parallel scans with computations of order  $\mathcal{O}(P \log(L))$ , which is negligible. Also, D is  $\mathcal{O}(HL)$ , which is much smaller than  $\mathcal{O}(LPH)$ , i.e., computation for B & C matrices or even  $\mathcal{O}(LH^2)$ , which is for the GLU layer. [21] uses GeLU and GLU non-linearities, which we replace with a linear layer. And, [48] described that GeLU consumes 14 FLOPs per operation. Moreover, GLU has twice as many FLOPs as a linear layer.

From Figure 3, we observe that for different state-to-hidden ratios, we get different energy numbers. For the EigenWorms dataset, the average spike rate per time step per block is 0.32. For a lower P/H ratio, we yield high energy efficiencies ( $\sim 120\times$ ). Even for a high ratio, our model block is  $\sim 20\times$  more energy-efficient than a LinOSS Block for EigenWorms. Our best performing model (as per Table 1) is **73.2** $\times$  more energy efficient than an equivalent LinOSS model.

## 4.2 Regression with spikes

None of the previously proposed spiking SSMs report performance on regression tasks [9, 20, 8]. In fact, most of the spiking deep learning research is focused on classification [5, 12]. Recently, a transformer-based method [33] has been proposed for spike-based regression of time series. But this approach is significantly limited (and deviates from present hardware-supported features[2]) due to its quadratic sequence length dependence bottleneck and computationally intensive FFT computations [20]. Unlike a transformer, SSMs have emerged as a powerful solution to the problem of such quadratic dependence on sequence length. To the best of our knowledge, for the first time, we report the regression performance of a spiking SSM for extremely long sequences (up to 50k length). Apparently, a spike-based output limits the output range for regression tasks, making it a difficult task for spiking neurons. Previously, a spike-free LI layer was shown to work for some datasets [49]. However, it is not scalable to the size of very long sequences due to the oversmoothing effect of the moving average. Another approach [33] translates spikes back into continuous values using a Linear layer. However, this method also leads to limited expressivity about the time steps. To mitigate these issues, we propose a kernel-based regression with a learnable kernel convolved over time, initialized with a decaying LI filter of fixed size. To find the best parameters, we apply Bayesian hyperparameter [46] search instead of the grid search with the same range of hyperparameters for a fair comparison. Subsequently, we ran a grid search on the best kernel size to ensure our model doesn't lose its representation power, nor oversmooths the outputs(see Table 5).

### 4.2.1 PPG-DaLiA Dataset Evaluation

To model very long-range interactions for regression tasks, we consider a 49920-length sequence following the processing and hyperparameter protocol as proposed in [42]. PPG-DaLiA is a multivariate time series regression dataset to predict heart rate using data collected from a wrist-worn device from 15 individuals for 150 minutes, sampled at 128Hz. We report the best MSE in the order of  $10^{-2}$  after applying Bayesian search for 15 runs, and applied the same hyperparameters for different discretizations. From Table 2, we observe that SHaRe-SSM models consistently outperform all first-order SSM variants, even after spiking in nature. Our best-performing model is SHaRe-SSM-IMEX, which outperforms Mamba by 0.0057 MSE, proving the energy-conserving nature of IMEX-discretization and our second-order resonating neuron representation power. Moreover, despite being energy efficient, we are only 0.0392 MSE lower than second-order SSMs.

Table 2: Mean and Standard Deviation reported for PPG-DaLiA dataset using hyperparameter protocol from [42] for the mean-squared error (MSE) across five training runs. For a clear differentiation, spiking neural networks are kept separately.

Model	SNN	MSE $\times 10^{-2}$
NRDE	N	9.90 $\pm$ 0.97
NCDE	N	13.54 $\pm$ 0.69
Log-NCDE	N	9.56 $\pm$ 0.59
LRU	N	12.17 $\pm$ 0.49
S5	N	12.63 $\pm$ 1.25
S6	N	12.88 $\pm$ 2.05
Mamba	N	10.65 $\pm$ 2.20
LinOSS-IMEX	N	7.5 $\pm$ 0.46
LinOSS-IM	N	6.4 $\pm$ 0.23
D-LinOSS	N	<b>6.16 <math>\pm</math> 0.73</b>
Ours (IM)	Y	11.27 $\pm$ 0.67
<b>Ours (IMEX)</b>	Y	<b>10.08 <math>\pm</math> 0.46</b>

### 4.2.2 Weather Dataset Evaluation

To test our model’s performance, we follow the hyperparameter protocol of [21] on a time series dataset that utilizes domain-specific preprocessing. We consider the most challenging task of 720-timestep prediction (hours) for the weather dataset from [50]. We report the best Mean Absolute Error with mean and standard deviation for our model on IM and IMEX discretizations. Also, we perform Bayesian search instead of grid search with the same hyperparameter protocol and report performance for both discretizations. SHaRe-SSM outperforms ANN transformer-based models[50, 51, 52] (Informer by 0.145). RNN-based models[53, 54] such as LSTnet by 0.171 and competitive performance with S4, with just a 0.008 drop. From Table 3, we notice that IMEX has a deviation lower than 0.003 compared to IM because of its energy-conserving properties.

Table 3: Mean and standard deviation (across five runs) of mean-absolute error (MAE) on the weather dataset while predicting future 720 timesteps. Hyperparameter protocol from [21]

Model	SNN	MAE
Informer	N	0.731
Informer <sup>†</sup>	N	0.741
LogTrans	N	0.773
Reformer	N	1.575
LSTMa	N	1.109
LSTnet	N	0.757
S4	N	0.578
LinOSS-IMEX	N	0.508
LinOSS-IM	N	0.528
D-LinOSS	N	0.486
<b>Ours (IMEX)</b>	Y	<b>0.586 <math>\pm</math> 0.001</b>
Ours (IM)	Y	0.586 $\pm$ 0.004

## 4.3 Ablation Studies

### 4.3.1 Heterogeneity Analysis

Given the established sensitivity of SSMs to initializations, SHaRe-SSM is incorporated with heterogeneities for components -  $\Omega$ , B, C, D matrices and  $\Delta t$ , of the HRF-SSM, and the thresholds for the C ( $\theta_C$ ), D ( $\theta_D$ ) matrices and, the encoder ( $\theta_{\text{encoder}}$ ). We did a detailed ablation study of the effect of each component’s heterogeneity on performance by making them homogeneous (initialized by a constant value across all neurons).

From Table 4, we observe that homogeneous initialization for neuronal thresholds leads to decreased performance. For homogeneous big step size, we see performance drop from 85.6 by 2.8% (See Table 4). Further, it drops down by 3.4% and 4.5% if the  $\Omega$  matrix and D matrix are initialized with frequencies to be homogeneously kept as one and zero, respectively, showing the importance of heterogeneous states in these networks. It drops by 5% if D is initialized with

Table 4: Ablation study - Studying the effect of making each component fixed (homogeneous) on the EigenWorms dataset using IMEX with the best parameters for five seeds.(Here,  $x^* = x^{-1/2}$ )

	Heterogeneity	Value	Accuracy
$\theta_{\text{encoder}}$	$\mathcal{U}(0, 1]$	1.0	$85.0 \pm 7.2$
$\Omega$	$\mathcal{U}(0, 1]$	1.0	$82.2 \pm 3.3$
$B$	$\mathcal{U}(-H^*, H^*)$	0.0	$85.0 \pm 4.5$
$C$	$\mathcal{U}(-P^*, P^*)$	0.0	$85.0 \pm 4.5$
$D$	$\mathcal{N}(0, 1)$	0.0	$80.5 \pm 4.6$
$\Delta t$	$\mathcal{U}(0, 1]$	1.0	$82.8 \pm 2.7$
$\theta_C$	$\mathcal{U}(0, 1]$	1.0	$83.3 \pm 3.9$
$\theta_D$	$\mathcal{U}(0, 1]$	1.0	$85.0 \pm 4.8$
$\Omega, B, C, D$	As Above	As Above	$85.5 \pm 4.1$
$\theta_C, \theta_D$	As Above	As Above	$83.9 \pm 5.1$
All	As Above	As Above	$85.5 \pm 4.1$
Only SSM	Default	Default	$87.2 \pm 3.3$

zero. This implies, it is desirable to mix the HRF output with the input spikes. Homogeneity in thresholds in the Encoder layer doesn't drop the performance much (only 0.6%), but for the thresholds of C and D, it drops by 1.7%, implying the importance of heterogeneous initialization for HRF neurons. We also noticed that complete homogenization of the model didn't alter the mean accuracy much; rather, the deviation nearly doubled. Interestingly, if we just consider the SSM layer in a SHaRe-SSM block, we observe a boost in model performance for EigenWorms by 1.6%, possibly because of higher representation power without the linear layer.

### 4.3.2 Kernel Size for Regression

For very long-range sequences, to avoid oversmoothing, but at the same time increasing the representation power of a linear decoder, we introduce convolving a filter. This can be thought of as similar to an LI filter with learnable parameters. We investigate kernel size on the best performing model from Table 3. From Table 5, we observe that for the 50k PPG-DaLiA dataset, a kernel size of 64 outperforms the 32 and 128 filters by an error of 0.005.

Table 5: Ablation on kernel size for regression task

Model	Kernel Size	MSE $\times 10^{-2}$
IMEX	32	$10.62 \pm 0.59$
	64	<b><math>10.08 \pm 0.46</math></b>
	128	$10.69 \pm 0.45$

## 5 Discussion

In this work, we investigate the plausibility of an integration of second-order spiking neurons in a state space model (SSM) framework. As part of it, we propose an energy-efficient second-order spiking SSM: SHaRe-SSM using harmonic resonate and fire neurons. In addition, we design a learnable encoder, decoder, and a compatible parallel scan method. SHaRe-SSM is fully spike-based without any GeLU or GLU. And, SHaRe-SSM is uniquely designed to achieve energy-efficient target variable modeling on very long sequences. We evaluate SHaRe-SSM on multiple such real-world datasets, ranging from 400 to almost 18k sequence lengths for classification. On average, SHaRe-SSM outperforms all first-order SSMs while being extremely energy efficient. Furthermore, we observe that SHaRe-SSM also outperforms first-order SSMs in an energy-efficient regression task on very long sequences of length 50k. In the future, we intend to work on Intel Loihi2 [2] implementation of SHaRe-SSM for edge AI applications.

## References

[1] Mike Davies, Andreas Wild, Garrick Orchard, Yulia Sandamirskaya, Gabriel A. Fonseca Guerra, Prasad Joshi, Philipp Plank, and Sumedh R. Risbud. Advancing neuromorphic computing with loihi: A survey of results and outlook. *Proceedings of the IEEE*, 109(5):911–934, 2021.

- [2] Sumit Bam Shrestha, Jonathan Timcheck, Paxon Frady, Leobardo Campos-Macias, and Mike Davies. Efficient video and audio processing with loihi 2. In *ICASSP 2024 - 2024 IEEE International Conference on Acoustics, Speech and Signal Processing (ICASSP)*, pages 13481–13485, 2024.
- [3] Filipp Akopyan, Jun Sawada, Andrew Cassidy, Rodrigo Alvarez-Icaza, John Arthur, Paul Merolla, Nabil Imam, Yutaka Nakamura, Pallab Datta, Gi-Joon Nam, Brian Taba, Michael Beakes, Bernard Brezzo, Jente B. Kuang, Rajit Manohar, William P. Risk, Bryan Jackson, and Dharmendra S. Modha. Truenorth: Design and tool flow of a 65 mw 1 million neuron programmable neuromorphic chip. *IEEE Transactions on Computer-Aided Design of Integrated Circuits and Systems*, 34(10):1537–1557, 2015.
- [4] Ole Richter, Chenxi Wu, Adrian M Whatley, German Köstinger, Carsten Nielsen, Ning Qiao, and Giacomo Indiveri. Dynap-se2: a scalable multi-core dynamic neuromorphic asynchronous spiking neural network processor. *Neuromorphic computing and engineering*, 4(1):014003, 2024.
- [5] Zhaokun Zhou, Yuesheng Zhu, Chao He, Yaowei Wang, Shuicheng YAN, Yonghong Tian, and Li Yuan. Spik-former: When spiking neural network meets transformer. In *The Eleventh International Conference on Learning Representations*, 2023.
- [6] Zhaokun Zhou, Jun Niu, Yang Zhang, Li Yuan, and Yuesheng Zhu. Spiking transformer with spatial-temporal spiking self-attention. In *ICASSP 2025 - 2025 IEEE International Conference on Acoustics, Speech and Signal Processing (ICASSP)*, pages 1–5, 2025.
- [7] Donghyun Lee, Yuhang Li, Youngeun Kim, Shiting Xiao, and Priyadarshini Panda. Spiking transformer with spatial-temporal attention, 2025.
- [8] Shuaijie Shen, Chao Wang, Renzhuo Huang, Yan Zhong, Qinghai Guo, Zhichao Lu, Jianguo Zhang, and Luziwei Leng. Spikingssms: Learning long sequences with sparse and parallel spiking state space models. *Proceedings of the AAAI Conference on Artificial Intelligence*, 39(19):20380–20388, Apr. 2025.
- [9] Matei-Ioan Stan and Oliver Rhodes. Learning long sequences in spiking neural networks. *Scientific Reports*, 14(1):21957, 2024.
- [10] A L Hodgkin and A F Huxley. A quantitative description of membrane current and its application to conduction and excitation in nerve. *J. Physiol.*, 117(4):500–544, August 1952.
- [11] Eugene M Izhikevich. Resonate-and-fire neurons. *Neural networks*, 14(6-7):883–894, 2001.
- [12] Saya Higuchi, Sebastian Kairat, Sander Bohte, and Sebastian Otte. Balanced resonate-and-fire neurons. In *Forty-first International Conference on Machine Learning*, 2024.
- [13] Maxime Fabre, Lyubov Dudchenko, and Emre Neftci. Structured state space model dynamics and parametrization for spiking neural networks. *arXiv preprint arXiv:2506.06374*, 2025.
- [14] Ashish Vaswani, Noam Shazeer, Niki Parmar, Jakob Uszkoreit, Llion Jones, Aidan N Gomez, Łukasz Kaiser, and Illia Polosukhin. Attention is all you need. In I. Guyon, U. Von Luxburg, S. Bengio, H. Wallach, R. Fergus, S. Vishwanathan, and R. Garnett, editors, *Advances in Neural Information Processing Systems*, volume 30. Curran Associates, Inc., 2017.
- [15] William Brandon, Mayank Mishra, Aniruddha Nrusimha, Rameswar Panda, and Jonathan Ragan-Kelley. Reducing transformer key-value cache size with cross-layer attention. In *The Thirty-eighth Annual Conference on Neural Information Processing Systems*, 2024.
- [16] Ali Behrouz, Peilin Zhong, and Vahab Mirrokni. Titans: Learning to memorize at test time. *arXiv preprint arXiv:2501.00663*, 2024.
- [17] Albert Gu, Karan Goel, and Christopher Ré. Efficiently modeling long sequences with structured state spaces. *arXiv preprint arXiv:2111.00396*, 2021.
- [18] Jimmy TH Smith, Andrew Warrington, and Scott W Linderman. Simplified state space layers for sequence modeling. *arXiv preprint arXiv:2208.04933*, 2022.
- [19] Albert Gu and Tri Dao. Mamba: Linear-time sequence modeling with selective state spaces. *arXiv preprint arXiv:2312.00752*, 2023.

- [20] Malyaban Bal and Abhronil Sengupta. P-spikessm: Harnessing probabilistic spiking state space models for long-range dependency tasks. In *The Thirteenth International Conference on Learning Representations*, 2025.
- [21] T. Konstantin Rusch and Daniela Rus. Oscillatory state-space models. In *The Thirteenth International Conference on Learning Representations*, 2025.
- [22] Jared Boyer, T. Konstantin Rusch, and Daniela Rus. Learning to dissipate energy in oscillatory state-space models, 2025.
- [23] Nabil Imam and Thomas A Cleland. Rapid online learning and robust recall in a neuromorphic olfactory circuit. *Nat. Mach. Intell.*, 2(3):181–191, March 2020.
- [24] Antonio Orvieto, Samuel L Smith, Albert Gu, Anushan Fernando, Caglar Gulcehre, Razvan Pascanu, and Soham De. Resurrecting recurrent neural networks for long sequences. In *International Conference on Machine Learning*, pages 26670–26698. PMLR, 2023.
- [25] T. Konstantin Rusch and Siddhartha Mishra. Coupled oscillatory recurrent neural network (co{rnn}): An accurate and (gradient) stable architecture for learning long time dependencies. In *International Conference on Learning Representations*, 2021.
- [26] T Konstantin Rusch and Siddhartha Mishra. Unicornn: A recurrent model for learning very long time dependencies. In *International Conference on Machine Learning*, pages 9168–9178. PMLR, 2021.
- [27] Samuel Lanthaler, T. Konstantin Rusch, and Siddhartha Mishra. Neural oscillators are universal. In *Thirty-seventh Conference on Neural Information Processing Systems*, 2023.
- [28] Badr AlKhamissi, Muhammad ElNokrashy, and David Bernal-Casas. Deep spiking neural networks with resonate-and-fire neurons. *arXiv preprint arXiv:2109.08234*, 2021.
- [29] Bojian Yin, Federico Corradi, and Sander M Bohtë. Accurate and efficient time-domain classification with adaptive spiking recurrent neural networks. *Nature Machine Intelligence*, 3(10):905–913, 2021.
- [30] Alexandre Bittar and Philip N Garner. A surrogate gradient spiking baseline for speech command recognition. *Frontiers in Neuroscience*, 16:865897, 2022.
- [31] Lucas Deckers, Laurens Van Damme, Werner Van Leekwijck, Ing Jyh Tsang, and Steven Latré. Co-learning synaptic delays, weights and adaptation in spiking neural networks. *Frontiers in Neuroscience*, 18:1360300, 2024.
- [32] Yulong Huang, Zunchang Liu, Changchun Feng, Xiaopeng Lin, Hongwei Ren, Haotian Fu, Yue Zhou, Hong Xing, and Bojun Cheng. Prf: Parallel resonate and fire neuron for long sequence learning in spiking neural networks. *arXiv preprint arXiv:2410.03530*, 2024.
- [33] Wenjie Wu, Dexuan Huo, and Hong Chen. Spikf: Spiking fourier network for efficient long-term prediction. In *Forty-second International Conference on Machine Learning*, 2025.
- [34] Svea Marie Meyer, Philipp Weidel, Philipp Plank, Leobardo Campos-Macias, Sumit Bam Shreshta, Philipp Stratmann, Jonathan Timcheck, and Mathis Richter. A diagonal structured state space model on loihi 2 for efficient streaming sequence processing. In *2025 Neuro Inspired Computational Elements (NICE)*, pages 1–9. IEEE, 2025.
- [35] Nicolas Perez-Nieves, Vincent C. H. Leung, Pier Luigi Dragotti, and Dan F. M. Goodman. Neural heterogeneity promotes robust learning. *Nature Communications*, 12(1):5791, October 2021. Publisher: Nature Publishing Group.
- [36] Hangchi Shen, Qian Zheng, Huamin Wang, and Gang Pan. Rethinking the membrane dynamics and optimization objectives of spiking neural networks. In *The Thirty-eighth Annual Conference on Neural Information Processing Systems*, 2024.
- [37] Maximilian Baronig, Romain Ferrand, Silvester Sabathiel, and Robert Legenstein. Advancing spatio-temporal processing in spiking neural networks through adaptation. *arXiv preprint arXiv:2408.07517*, 2024.
- [38] Emre O Neftci, Hesham Mostafa, and Friedemann Zenke. Surrogate gradient learning in spiking neural networks: Bringing the power of gradient-based optimization to spiking neural networks. *IEEE Signal Processing Magazine*, 36(6):51–63, 2019.

- [39] V I Arnold. *Mathematical methods of classical mechanics*. Graduate texts in mathematics. Springer, New York, NY, December 2010.
- [40] Peter M Kogge and Harold S Stone. A parallel algorithm for the efficient solution of a general class of recurrence equations. *IEEE Transactions on Computers*, 22(8):786–793, 1973.
- [41] Guy E Blelloch. Prefix sums and their applications. 1990.
- [42] Benjamin Walker, Andrew Donald Mcleod, Tiexin Qin, Yichuan Cheng, Haoliang Li, and Terry Lyons. Log neural controlled differential equations: The lie brackets make a difference. In *Proceedings of the 41st International Conference on Machine Learning*, volume 235 of *Proceedings of Machine Learning Research*, pages 49822–49844. PMLR, 21–27 Jul 2024.
- [43] Anthony Bagnall, Hoang Anh Dau, Jason Lines, Michael Flynn, James Large, Aaron Bostrom, Paul Southam, and Eamonn Keogh. The uea multivariate time series classification archive, 2018. *arXiv preprint arXiv:1811.00075*, 2018.
- [44] James Morrill, Cristopher Salvi, Patrick Kidger, and James Foster. Neural rough differential equations for long time series. In *International Conference on Machine Learning*, pages 7829–7838. PMLR, 2021.
- [45] Patrick Kidger, James Morrill, James Foster, and Terry Lyons. Neural controlled differential equations for irregular time series. *Advances in neural information processing systems*, 33:6696–6707, 2020.
- [46] Takuya Akiba, Shotaro Sano, Toshihiko Yanase, Takeru Ohta, and Masanori Koyama. Optuna: A next-generation hyperparameter optimization framework. In *The 25th ACM SIGKDD International Conference on Knowledge Discovery & Data Mining*, pages 2623–2631, 2019.
- [47] Mark Horowitz. 1.1 computing’s energy problem (and what we can do about it). In *2014 IEEE international solid-state circuits conference digest of technical papers (ISSCC)*, pages 10–14. IEEE, 2014.
- [48] Weihao Yu, Chenyang Si, Pan Zhou, Mi Luo, Yichen Zhou, Jiashi Feng, Shuicheng Yan, and Xinchao Wang. Metaformer baselines for vision. *IEEE Transactions on Pattern Analysis and Machine Intelligence*, 46(2):896–912, 2023.
- [49] Alexander Henkes, Jason K Eshraghian, and Henning Wessels. Spiking neural networks for nonlinear regression. *R. Soc. Open Sci.*, 11(5):231606, May 2024.
- [50] Haoyi Zhou, Shanghang Zhang, Jieqi Peng, Shuai Zhang, Jianxin Li, Hui Xiong, and Wancai Zhang. Informer: Beyond efficient transformer for long sequence time-series forecasting. In *Proceedings of the AAAI conference on artificial intelligence*, volume 35, pages 11106–11115, 2021.
- [51] Shiyang Li, Xiaoyong Jin, Yao Xuan, Xiyong Zhou, Wenhui Chen, Yu-Xiang Wang, and Xifeng Yan. Enhancing the locality and breaking the memory bottleneck of transformer on time series forecasting. *Advances in neural information processing systems*, 32, 2019.
- [52] Nikita Kitaev, Łukasz Kaiser, and Anselm Levskaya. Reformer: The efficient transformer. *arXiv preprint arXiv:2001.04451*, 2020.
- [53] Dzmitry Bahdanau, Kyunghyun Cho, and Yoshua Bengio. Neural machine translation by jointly learning to align and translate. *arXiv preprint arXiv:1409.0473*, 2014.
- [54] Guokun Lai, Wei-Cheng Chang, Yiming Yang, and Hanxiao Liu. Modeling long-and short-term temporal patterns with deep neural networks. In *The 41st international ACM SIGIR conference on research & development in information retrieval*, pages 95–104, 2018.

## A Technical Appendix

### A.1 Background Theory

To study the theoretical properties of a second-order ODE in SHaRe-SSM, we take inspiration from [21]. Our model, just like their model, can be formulated as energy-conserving and with dissipative attributes.

### A.1.1 Implicit Discretization (IM):

We consider the implicit (backward Euler) discretization of a second-order system involving a position-like state  $u_n$  and a velocity-like state  $v_n$ , similar to [21]. The implicit scheme is known to introduce additional dissipative terms, which contribute to the stability of the dynamics, particularly in the presence of stiffness.

The discretized updates are given by:

$$\begin{aligned} u_n &= u_{n-1} + \Delta t (-\Omega v_n + Bx_n), \\ v_n &= v_{n-1} + \Delta t u_n, \end{aligned}$$

where  $\Omega$  is a diagonal matrix of oscillation frequencies and  $B$  is an input projection matrix. Note that both  $u_n$  and  $v_n$  are evaluated at the future timestep, in contrast to explicit methods.

Letting the concatenated state be  $s_n$ , the above system can be written compactly as:

$$Ms_n = s_{n-1} + F_n,$$

where

$$M = \begin{pmatrix} I & \Delta t \Omega \\ -\Delta t I & I \end{pmatrix}, \quad F_n = \begin{pmatrix} \Delta t Bx_n \\ 0 \end{pmatrix}.$$

To obtain an explicit update rule, we algebraically solve the coupled system by introducing the matrix inverse  $S = (I + \Delta t^2 \Omega)^{-1}$ . Substituting and simplifying yields:

$$s_n = M^{\text{IM}} s_{n-1} + F_n^{\text{IM}}, \quad (6)$$

where

$$M^{\text{IM}} = \begin{pmatrix} S & -S\Delta t \Omega \\ S\Delta t & S \end{pmatrix}, \quad F_n^{\text{IM}} = \begin{pmatrix} S\Delta t Bx_n \\ S\Delta t^2 Bx_n \end{pmatrix}.$$

This formulation highlights the stabilizing effect of the implicit method: the matrix  $S = (I + \Delta t^2 \Omega)^{-1}$  is a Schur complement that acts as a preconditioner that suppresses high-frequency components. Consequently, the eigenvalues of  $M^{\text{IM}}$  remain bounded within the unit circle for a wide range of  $\Delta t$ , leading to improved numerical stability. The Schur complement can be computed in  $\mathcal{O}(m)$  instead of the typical  $\mathcal{O}(m^3)$  operations using Gauss-Jordan elimination.

**Proposition A.1.** *Let  $M^{\text{IM}} \in \mathbb{R}^{2p \times 2p}$  be the hidden-to-hidden weight matrix of the implicit model SHaRe-SSM-IM (6). We assume that  $\Omega_j \geq 0$  for all diagonal elements  $j = 1, \dots, p$  of  $\Omega$ , and further that  $\Delta t > 0$ . Then, the complex eigenvalues of  $M^{\text{IM}}$  are given as,*

$$\lambda_{j1,2} = \frac{1}{1 + \Delta t^2 \Omega_j} \pm \Delta t \frac{\sqrt{\Omega_j}}{1 + \Delta t^2 \Omega_j}$$

with  $\lambda_{j1} = \overline{\lambda_{j2}}$ . Moreover, the spectral radius  $\rho(M^{\text{IM}})$  is bounded by 1, i.e.,  $|\lambda_j| \leq 1$  for all  $j = 1, \dots, p$ .

*Proof.* The matrix  $M^{\text{IM}} \in \mathbb{R}^{2p \times 2p}$  is defined as

$$M^{\text{IM}} = \begin{bmatrix} S & -\Delta t \Omega S \\ \Delta t S & S \end{bmatrix},$$

where  $S = (I + \Delta t^2 \Omega)^{-1}$ , and  $\Omega \in \mathbb{R}^{p \times p}$  is diagonal with non-negative entries  $\Omega_j \geq 0$  for all  $j = 1, \dots, p$ .

To determine the eigenvalues, we compute the characteristic polynomial:

$$\det(M^{\text{IM}} - \lambda I) = \begin{vmatrix} S - \lambda I & -\Delta t \Omega S \\ \Delta t S & S - \lambda I \end{vmatrix}.$$

Using block Gaussian elimination, we subtract  $(\Delta t S)(S - \lambda I)^{-1}(-\Delta t \Omega S)$  from the lower-right block, giving

$$= \det(S - \lambda I) \cdot \det(S - \lambda I + \Delta t^2 \Omega S^2 (S - \lambda I)^{-1}).$$

Since  $S$  and  $\Omega$  are diagonal and commute, this expression decouples elementwise. Let  $s_j = \frac{1}{1 + \Delta t^2 \Omega_j}$  be the  $j$ -th diagonal element of  $S$ . Then for each  $j = 1, \dots, p$ , the scalar characteristic equation becomes

$$(s_j - \lambda)^2 + \Delta t^2 \Omega_j s_j^2 = 0.$$

Solving this quadratic gives the eigenvalue pair

$$\lambda_{j1,2} = s_j \pm i \Delta t s_j \sqrt{\Omega_j},$$

where  $\lambda_{j1} = \overline{\lambda_{j2}}$ , i.e., the pair are complex conjugates.

To compute their magnitude:

$$|\lambda_{j1,2}|^2 = s_j^2(1 + \Delta t^2 \Omega_j) = \frac{1}{1 + \Delta t^2 \Omega_j} \leq 1.$$

Hence, all eigenvalues lie on or inside the unit circle in the complex plane, and the spectral radius satisfies  $\rho(M^{IM}) \leq 1$ , as claimed.  $\square$

**Proposition A.2.** Let  $\{\lambda_j\}_{j=1}^{2p}$  denote the eigenvalues of the hidden-to-hidden matrix  $M^{IM} \in \mathbb{R}^{2p \times 2p}$  of the SHaRe-SSM-IM model (6). Suppose the diagonal entries of  $\Omega \in \mathbb{R}^{p \times p}$  are independently drawn as  $\Omega_j \sim \mathcal{U}([0, \Omega_{\max}])$ , with  $\Omega_{\max} > 0$ . Then, the  $N$ -th moment of the magnitude of the eigenvalues is given by

$$\mathbb{E}(|\lambda_j|^N) = \frac{(1 + \Delta t^2 \Omega_{\max})^{1 - \frac{N}{2}} - 1}{\Delta t^2 \Omega_{\max} (1 - \frac{N}{2})}, \quad \forall j = 1, \dots, 2p.$$

*Proof.* From Proposition A.1, each eigenvalue of  $M^{IM}$  has magnitude

$$|\lambda_j| = \sqrt{s_j} = \sqrt{\frac{1}{1 + \Delta t^2 \Omega_j}}.$$

The  $N$ -th moment of the magnitude is thus.

$$\mathbb{E}(|\lambda_j|^N) = \mathbb{E} \left[ \left( \frac{1}{1 + \Delta t^2 \Omega_j} \right)^{\frac{N}{2}} \right].$$

Applying the law of the unconscious statistician and the uniform distribution of  $\Omega_j \sim \mathcal{U}([0, \Omega_{\max}])$ , we write:

$$\mathbb{E}(|\lambda_j|^N) = \frac{1}{\Omega_{\max}} \int_0^{\Omega_{\max}} (1 + \Delta t^2 x)^{-\frac{N}{2}} dx.$$

Substituting  $u = 1 + \Delta t^2 x$ , so that  $du = \Delta t^2 dx$ , the limits change from  $x = 0$  to  $x = \Omega_{\max}$ , corresponding to  $u = 1$  to  $u = 1 + \Delta t^2 \Omega_{\max}$ . The integral becomes:

$$\mathbb{E}(|\lambda_j|^N) = \frac{1}{\Delta t^2 \Omega_{\max}} \int_1^{1 + \Delta t^2 \Omega_{\max}} u^{-\frac{N}{2}} du.$$

This evaluates to

$$\mathbb{E}(|\lambda_j|^N) = \frac{(1 + \Delta t^2 \Omega_{\max})^{1 - \frac{N}{2}} - 1}{\Delta t^2 \Omega_{\max} (1 - \frac{N}{2})},$$

$\square$

We can observe from proposition A.2 that even though the spectral radius of eigenvalues is smaller than one (proposition A.1), it is large enough to capture long-range dependencies even for very long-range sequences, even for  $\Omega_{\max} = 1, \Delta t = 1$ . Hence, we initialize  $\Omega_j \sim \mathcal{U}([0, 1])$ ,  $\Delta t_j \sim \mathcal{U}([0, 1])$

### A.1.2 Implicit-Explicit Discretization (IMEX):

We also utilize an implicit-explicit (IMEX) scheme for discretizing the second-order harmonic oscillator system, similar to [21]. IMEX methods treat the stiff terms implicitly and the non-stiff or input terms explicitly, resulting in a balanced scheme that enables stable yet undamped oscillations. As shown in [21], such schemes preserve the total energy of the system and therefore are particularly well-suited for learning long-range sequential patterns without introducing artificial dissipation.

The update equations under the IMEX discretization are given by:

$$\begin{aligned} u_n &= u_{n-1} + \Delta t (-\Omega v_{n-1} + Bx_n), \\ v_n &= v_{n-1} + \Delta t u_n, \end{aligned}$$

where the velocity update depends implicitly on the newly computed  $u_n$ , while the force term  $-\Omega v_{n-1} + Bx_n$  is evaluated using previous state values.

Defining the state vector as  $s_n$ , we can rewrite the update in matrix form:

$$Ms_n = M_1 s_{n-1} + F_n,$$

where the matrices  $M$ ,  $M_1$ , and input vector  $F_n$  are:

$$M = \begin{pmatrix} I & 0 \\ -\Delta t I & I \end{pmatrix}, M_1 = \begin{pmatrix} I & -\Delta t \Omega \\ 0 & I \end{pmatrix}, F_n = \begin{pmatrix} \Delta t Bx_n \\ 0 \end{pmatrix}.$$

Multiplying both sides by  $M^{-1}$  yields the closed-form update:

$$s_n = M^{\text{IMEX}} s_{n-1} + F_n^{\text{IMEX}}, \quad (7)$$

where the transition matrix and input vector are given by:

$$M^{\text{IMEX}} = \begin{pmatrix} I & -\Delta t \Omega \\ \Delta t I & I - \Delta t^2 \Omega \end{pmatrix}, \quad F_n^{\text{IMEX}} = \begin{pmatrix} \Delta t Bx_n \\ \Delta t^2 Bx_n \end{pmatrix}.$$

**Proposition A.3.** *Let  $M^{\text{IMEX}} \in \mathbb{R}^{2p \times 2p}$  be the hidden-to-hidden weight matrix of the implicit-explicit model SHaRe-SSM-IMEX (7). Suppose that  $\Omega \in \mathbb{R}^{p \times p}$  is diagonal with strictly positive entries  $\Omega_j > 0$  for all  $j = 1, \dots, p$ , and that the time step satisfies  $0 < \Delta t \leq \max_j \left( \frac{2}{\sqrt{\Omega_j}} \right)$ . Then, the eigenvalues of  $M^{\text{IMEX}}$  are given by*

$$\lambda_{j1,2} = \frac{1}{2}(2 - \Delta t^2 \Omega_j) \pm \frac{1}{2} \sqrt{\Delta t^2 \Omega_j (4 - \Delta t^2 \Omega_j)},$$

with  $\lambda_{j1} = \overline{\lambda_{j2}}$ . Moreover, the eigenvalues lie on the complex unit circle, i.e.,  $|\lambda_j| = 1, \quad \forall j = 1, \dots, p$ .

*Proof.* The matrix  $M^{\text{IMEX}} \in \mathbb{R}^{2p \times 2p}$  has the block form

$$M^{\text{IMEX}} = \begin{bmatrix} I & -\Delta t \Omega \\ \Delta t I & I \end{bmatrix} \begin{bmatrix} (I + \Delta t^2 \Omega)^{-1} & 0 \\ 0 & (I + \Delta t^2 \Omega)^{-1} \end{bmatrix},$$

So the effective system matrix becomes

$$M^{\text{IMEX}} = \begin{bmatrix} S & -\Delta t \Omega S \\ \Delta t S & S \end{bmatrix}, \quad \text{where } S = (I + \Delta t^2 \Omega)^{-1}.$$

We analyze the characteristic polynomial:

$$\det(M^{\text{IMEX}} - \lambda I) = \begin{vmatrix} S - \lambda I & -\Delta t \Omega S \\ \Delta t S & S - \lambda I \end{vmatrix}.$$

Using block elimination, we simplify:

$$= \det(S - \lambda I)^2 + \Delta t^2 \Omega S^2.$$

Since all matrices are diagonal, the problem decouples elementwise. Let  $s_j = \frac{1}{1 + \Delta t^2 \Omega_j}$  for each  $j = 1, \dots, p$ . Then, for each  $j$ , the characteristic polynomial becomes

$$\lambda^2 - (2s_j)\lambda + (s_j^2 + \Delta t^2 \Omega_j s_j^2) = \lambda^2 - (2 - \Delta t^2 \Omega_j)\lambda + 1 = 0.$$

Solving this gives the eigenvalue pair

$$\lambda_{j1,2} = \frac{1}{2}(2 - \Delta t^2 \Omega_j) \pm \frac{1}{2} \sqrt{\Delta t^2 \Omega_j (4 - \Delta t^2 \Omega_j)}.$$

To show  $|\lambda_{j1,2}| = 1$ , we consider two cases:

1. **If**  $\Delta t^2 \Omega_j = 4$ , then the square root vanishes and

$$\lambda_{j_1} = \lambda_{j_2} = -1, \quad |\lambda_{j_{1,2}}| = 1.$$

2. **If**  $\Delta t^2 \Omega_j < 4$ , then the eigenvalues are complex conjugates. Their squared magnitude is

$$\begin{aligned} |\lambda_{j_{1,2}}|^2 &= \left( \frac{2 - \Delta t^2 \Omega_j}{2} \right)^2 + \left( \frac{1}{2} \sqrt{\Delta t^2 \Omega_j (4 - \Delta t^2 \Omega_j)} \right)^2 \\ &= \frac{(2 - \Delta t^2 \Omega_j)^2 + \Delta t^2 \Omega_j (4 - \Delta t^2 \Omega_j)}{4} \\ &= \frac{4 - 4\Delta t^2 \Omega_j + \Delta t^4 \Omega_j^2 + 4\Delta t^2 \Omega_j - \Delta t^4 \Omega_j^2}{4} = 1. \end{aligned}$$

Thus, in both cases,  $|\lambda_{j_{1,2}}| = 1$ , completing the proof. □